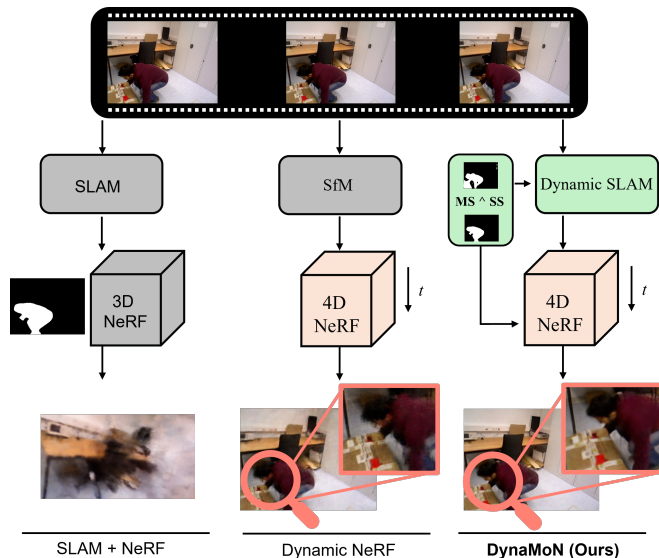


DynaMoN: Motion-Aware Fast and Robust Camera Localization for Dynamic Neural Radiance Fields

Nicolas Schischka^{1*}, Hannah Schieber^{2,4*}, Mert Asim Karaoglu^{1,3*}, Melih Gorgulu^{1*}, Florian Grötzner¹, Alexander Ladikos³, Daniel Roth², Nassir Navab^{1,5}, and Benjamin Busam¹

Abstract—The accurate reconstruction of dynamic scenes with neural radiance fields is significantly dependent on the estimation of camera poses. Widely used structure-from-motion pipelines encounter difficulties in accurately tracking the camera trajectory when faced with separate dynamics of the scene content and the camera movement. To address this challenge, we propose **Dynamic Motion-Aware Fast and Robust Camera Localization for Dynamic Neural Radiance Fields (DynaMoN)**. DynaMoN utilizes semantic segmentation and generic motion masks to handle dynamic content for initial camera pose estimation and statics-focused ray sampling for fast and accurate novel-view synthesis. Our novel iterative learning scheme switches between training the NeRF and updating the pose parameters for an improved reconstruction and trajectory estimation quality. The proposed pipeline shows significant acceleration of the training process. We extensively evaluate our approach on two real-world dynamic datasets, the TUM RGB-D dataset and the BONN RGB-D Dynamic dataset. DynaMoN improves over the state-of-the-art both in terms of reconstruction quality and trajectory accuracy. We plan to make our code public to enhance research in this area.



I. INTRODUCTION

Enabling novel view synthesis on dynamic scenes often requires multi-camera setups [1]. However, everyday dynamic scenes are often captured by one single moving camera, restricting the field of view [1]. In Simultaneous Localization and Mapping (SLAM) pipelines, multiple scene representations can be used. Commonly used explicit voxel and surfel representations are complemented by implicit truncated signed distance fields (TSDF) or neural radiance fields (NeRF). The latter allows the rendering of photorealistic novel views from new, reasonable camera positions [2], [3]. While many are restricted to static scenes, dynamic NeRF [4], [5], [6], [7] allows novel view synthesis for dynamic scenes.

To enable novel view synthesis using NeRF, accurate camera poses, usually retrieved via COLMAP [8] or the Apple ARKit, are essential. The structure-from-motion (SfM)-based

Fig. 1. NeRF-SLAM approaches rely on static scenes (left). Approaches such as InstantNGP [3] can be used to mask out dynamic scene content [2], [11] (left). Still, when using the masking, the scene representation lacks quality (left). Fully dynamic NeRF provides an implicit 4D (3D+time) representation; however, it relies on offline SfM, which can suffer in the presence of considerable motion (center). We consider dynamics via our motion-based segmentation (MS) and semantic segmentation (SS) already in the camera localization (right) and further during novel view synthesis. This enables a more robust camera tracking and novel view synthesis with a higher quality (ours, right).

approach often demands hours of computation to estimate reasonable camera poses and is challenged by large-scale dynamic scenes. To overcome the limitation of slow SfM approaches, recent works combined SLAM and NeRF [9], [10], [11], [2]. SLAM provides faster results for the camera trajectory than classic SfM. However, by nature, scenes are more often dynamic than static. Existing NeRF-SLAM [9], [10], [11], [2] methods assume a static scene which poses difficulties when dynamic scene content is present as shown in Fig 1. ¹

In this paper, we present DynaMoN, a motion-aware camera localization and visualization approach that can handle highly dynamic scenes in camera pose retrieval and dynamic scene representation. We utilize semantic segmentation and generic motion masks during our camera localization process to enable robust tracking of the camera path in a dynamic en-

*equal contribution

¹Mert Asim Karaoglu, Benjamin Busam, Nassir Navab, Nicolas Schischka, Melih Gorgulu, Florian Grötzner are with Technical University of Munich, Munich, Germany mert.karaoglu@tum.de

²Daniel Roth and Hannah Schieber are with Human-Centered Computing and Extended Reality Lab, Technical University of Munich, School of Medicine and Health, Klinikum rechts der Isar, Orthopedics and Sports Orthopedics, Munich, Germany hannah.schieber@tum.de

³Mert Asim Karaoglu and Alexander Ladikos are with ImFusion GmbH, Munich, Germany

⁴Hannah Schieber is with the Friedrich-Alexander Universität Erlangen-Nürnberg, Erlangen, Germany

⁵Nassir Navab is with Johns Hopkins University, Baltimore, MD, USA

¹This work has been submitted to the IEEE for possible publication. Copyright may be transferred without notice, after which this version may no longer be accessible.

vironment. These masks are further utilized for ray sampling to train an efficient dynamic NeRF, based on HexPlane [4], that refines the initial camera poses, leading to improved reconstruction quality in scenes with strong motions.

We conduct experiments on two challenging datasets, namely the dynamic subset of the TUM RGB-D [12] and the BONN RGB-D Dynamic [13] dataset. The considered masking in DynaMoN allows us to outperform existing approaches in terms of the absolute trajectory error and novel view synthesis results on these datasets.

II. RELATED WORK

As DynaMoN is a combination of dynamic NeRF with fast and robust motion-aware camera localization, we group related work in topics for camera localization and their employment for novel view synthesis and neural representation for dynamic scenes.

A. Camera Localization and Scene Dynamics

SfM and SLAM [14], [15], [16], [17] are arguably the two most common approaches for robust camera localization. More specifically, SLAM often targets real-time localization of a camera coupled with mapping. In addition to visual information, some approaches can utilize complementary sensory signals such as depth images and IMU data to further improve the accuracy. A common branch of work employs ORB descriptors to build a 3D map and track the camera [14], [17], [15].

In addition to classical or partially learnable SLAM approaches, Teed and Deng [16] introduce an end-to-end learnable method. Their approach, termed DROID-SLAM, consists of a dense bundle adjustment layer that enables recurrent iterative updates of camera poses and pixel-wise depth.

Typical camera localization approaches rely on a static scene assumption. However, natural scenes are often dynamic [18], [19], [20], [21]. To address this, Yu et al. [18] introduce a dynamic SLAM approach building upon ORB-SLAM2 [17]. Their DS-SLAM integrates a semantic segmentation network and a moving consistency check in the tracking process. Rünz et al. [22] enrich RGB-D SLAM with object-awareness and semantic segmentation capabilities, while DynaSLAM [23] combines geometric and deep learning-based segmentation to mask dynamic objects in an attempt to ignore them for mapping. Others split the scene into dynamic and static parts. Dai et al. [20] build upon ORB-SLAM2 [17] and introduce a semantic segmentation using point correlation for this split and Ye et al. [21] divide the scene representation in a static flow field and a dynamic flow field. Yu et al. [24] combine semantic segmentation with optical flow to remove dynamic keypoints achieving a higher robustness compared to ORB-SLAM2.

Following this idea, we also split the scene into static parts and dynamic content using predicted segmentation masks.

B. Camera Localization and NeRF

With the retrieved camera poses, a captured environment can be represented in 3D. Aside from explicit maps, an implicit scene representation can be established using a multilayer perceptron (MLP) [25]. Mildenhall et al. [25] introduce the use of an MLP as a neural representation for novel view synthesis, denoted as NeRF. The implicit representation is regressed by a photometric comparison of rendered views with input images. This allows the synthesis of photorealistic images from novel viewpoints at the cost of the requirement for accurate camera poses during training, typically captured by computationally intensive SfM with COLMAP [8]. An efficient alternative to SfM is the use of SLAM to retrieve camera poses.

In this regard, Sucar et al. [26] propose the usage of an MLP as scene representation in a SLAM framework and Zhu et al. [9] arrange multiple NeRFs in a hierarchical feature grid to learn both camera pose and scene representation. NICER-SLAM [10] introduces a similar approach for RGB input with estimated depth. Others purely rely on RGB and combine SLAM and NeRF [2], [11] utilizing hash-based InstantNGP [3] for scene representation. NeRF-SLAM [2] adapts the initial Droid-SLAM [16] framework and OrbeeZ-SLAM [11] leverages visual odometry [17].

To incorporate efficient pose estimation, we also rely on design choices of recent SLAM frameworks; however, we combine them with computationally efficient proposals [4] for neural radiance fields.

C. Neural Representation of Dynamic Scenes

Our world is inherently dynamic which violates commonly used static scene assumptions [9], [10], [26], [11], [2], [3], [25]. To represent dynamics in a NeRF [27], [28], the use of grid structures became popular [4], [5]. HexPlane [4] utilizes a 4D space-time grid divided into six feature planes. The feature vector is a 4D point in space-time projected onto each feature plane. Similarly, Tensor4d [5] builds upon a 4D tensor field using time-aware volumes projected onto nine 2D planes. TiNeuVox [7] represents dynamic scenes using time-aware voxel features to enable faster training.

Optimizing for both camera poses and view synthesis can improve results in static scenes [29], [30], [31], [32], [33]. Liu et al. [34] therefore introduce such an optimization for a dynamic environment. To model this, they use one static and one dynamic NeRF.

We, in contrast, split the problem into the differentiation of static and dynamic content already used for camera pose estimation. The dynamic environment is then represented by a dynamic, 4D NeRF calculated upon the camera poses from the static scene components, while further refining these poses based on the static parts of the images.

III. METHOD

We consider our input to be an RGB video captured in a dynamic environment using a single monocular moving camera without pose knowledge. This leads to two objectives:

first, estimating the camera pose, and second, reconstructing the scene, which may comprise some deformation. We leverage masks to separate the scene dynamics from the static background for the former and utilize a 4D spatio-temporal neural representation for the latter. This allows to optimize for novel view synthesis while refining initial camera poses.

A. Robust Camera Localization in Dynamic Environments

Novel view synthesis methods commonly employ rigid SfM, often COLMAP [8], for camera pose estimation. This assumes a static scene instead of dynamic scenes.

To cope with dynamics, it is possible to add binary masks to remove non-static regions. However, the high computation time of SfM approaches remains a drawback. In our approach, we target both robustness against dynamic scenes and a more efficient solution for pose estimation for dynamic moving cameras. Our underlying architecture is based on DROID-SLAM [16]. While it incorporates elements to cope with a certain level of scene dynamics, we found it can be improved by eliminating the contribution of the non-static regions for camera tracking. We do this by generating binary dynamics masks for each frame, which are combinations of semantic (M_{SS}) and motion masks (M_{MS}).

The semantic mask follows the paradigm that in real videos, the most prominent source of motion is often an object of known class. We, therefore, define $M_{SS} = \mathbf{1}(x > 0) \circ \sum_i M_{SS}(i)$ for all defined semantic classes $i \in S$ of the set S with the indicator function being 1 for positive values. Additional moving objects are covered through a motion mask M_{MS} . One example is depicted by the moving box in Fig 2. Following DytanVO [35], our motion masks are generated using a CNN with the previous image, the forward optical flow and the estimated camera motion as input to iteratively refine the mask along with updates of the relative motion between frames. Instead of random initialization, we begin with the motion mask of the previous frame to improve stability and lower the number of iterations in our refinement. We combine both masks as $M = \mathbf{1}(x > 0) (M_{SS} + M_{MS})$.

B. Neural Dynamic Scenes

Our scene representation builds on a state-of-the-art dynamic NeRF, HexPlane [4]. Targeting efficient optimization, fast rendering and high reconstruction quality, HexPlane [4] utilizes TensoRF [36] and constructs a 4D representation with three spatial and one temporal axes to create feature planes with their pairwise combinations to be the input of their tiny MLP. The grid size of each axis is governed in a coarse-to-fine fashion along the training to improve convergence and naturally regularizes the local neighborhoods. For optimization, we follow the original NeRF ray casting and apply the pixel-wise photometric loss between the rendered RGB values C and the ground truth values \hat{C} , supported by a total variation regularization as:

$$\mathcal{L} = \frac{1}{|\mathcal{R}|} \sum_{\mathbf{r} \in \mathcal{R}} \|C(\mathbf{r}) - \hat{C}(\mathbf{r})\|_2^2 + \lambda_{TV} \mathcal{L}_{TV}. \quad (1)$$

While \mathcal{R} represents the sampled rays, \mathcal{L}_{TV} and λ_{TV} depict the total variation regularization and its weight.

C. Pose Refinement and Training Strategy

We utilize eqn. (1) as the objective function for training both the NeRF and refining the camera poses. For the latter, we employ an alternating training strategy in which every 5 000 iterations, the parameters to be optimized are switched between the radiance field and the pose parameters. To improve the accuracy and robustness of the optimization, during the pose refinement phase, we constrain the sampled rays, \mathcal{R} , contributing to the loss to be elements of the static regions designated by the dynamics masks. Furthermore, we also use the same masks to ensure that the total variation regularization is imposed only on the static components. As the amount of non-dynamic sampled rays can vary from image to image, we scale the learning rate η_s output by a learning rate scheduler by the fraction of static pixels in the image to keep the optimization steps in the same magnitude:

$$\eta = \eta_s * \frac{n_{static}}{n_{static} + n_{dynamic}}, \quad (2)$$

where n_{static} and $n_{dynamic}$ represent the number of static and dynamic pixels in the image and η is the learning rate used for the pose refinement.

IV. EVALUATION

To evaluate our approach, we consider two aspects. First, we consider the translational and rotational absolute trajectory error (ATE) [39] using root mean square error (RMSE) in meters and degrees. Second, we analyze the rendering quality of the novel dynamic views by reporting PSNR and SSIM [40] values.

A. Datasets

To assess DynaMoN, we compare both the camera localization and the novel view synthesis part with state-of-the-art approaches on two challenging datasets.

a) *TUM RGB-D - Dynamic subset* [12]: The TUM RGB-D dataset has a resolution of 640×480 . While the dataset mainly focuses on static parts, five sequences were rated *slightly dynamic* and four *highly dynamic*.

b) *BONN RGB-D Dynamic* [13]: The BONN RGB-D Dynamic dataset consists of 24 dynamic sequences and two static sequences. The number of recordings per scene varies. The images have a resolution of 640×480 .

For the novel view synthesis results, we follow the usual splitting using every eighth frame of the TUM RGB-D [12] dataset and BONN RGB-D Dynamic [13] dataset for testing.

B. Implementation Details

We implemented our approach in Python using PyTorch and evaluated it on one single workstation (Intel i9-10980XE CPU, NVIDIA GeForce RTX 3090 GPU 24GB, and 128GB RAM) unless otherwise specified.

For semantic masking, we use DeepLabV3 [42] with a ResNet50-backbone [43] trained on the large-scale COCO dataset [44] and use human masks. For motion masking, we use the trained model of DytanVO [35]. In practice, initialized with the motion mask of the previous frame, we

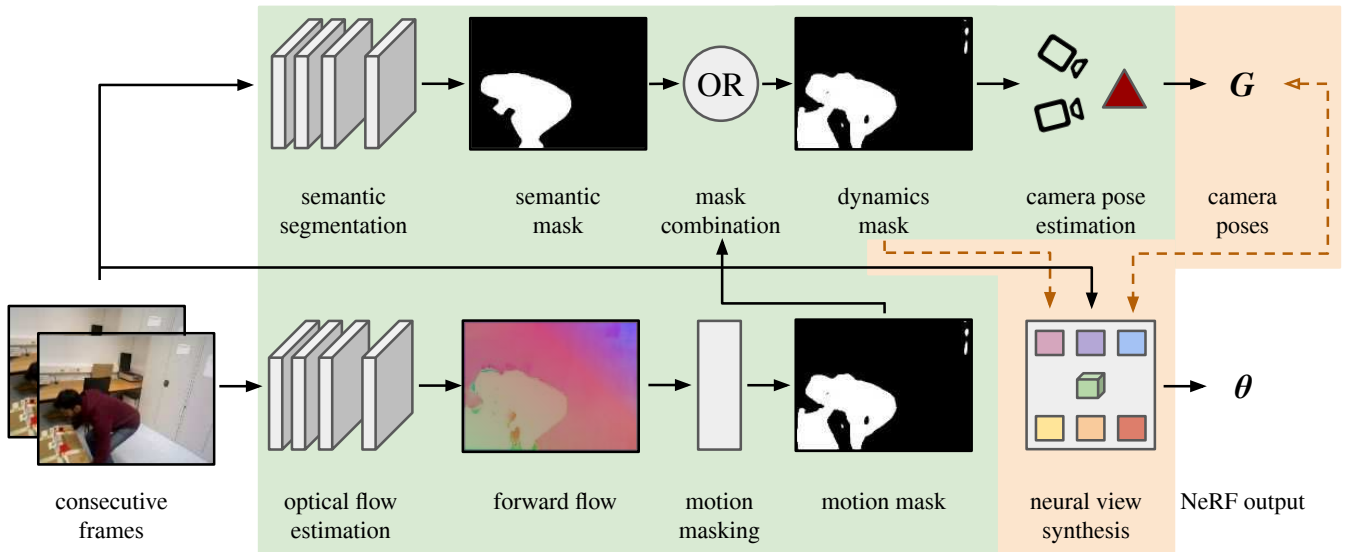


Fig. 2. **DynaMoN architecture.** DynaMoN retrieves consecutive RGB frames and applies semantic segmentation ($M_{ss} \rightarrow S_{S_i}$) and motion masks ($M_{MS} \rightarrow S_{M_i}$) on these input frames (I). Combining these masks (OR), we enable a motion-aware, fast and robust camera pose estimation. Based on the predicted camera poses G , we produce a time-dependent output (Θ) using dynamic NeRF. During NeRF training, we utilize the previously computed masks to refine the camera poses (dashed lines). Dashed lines represent iterative updates on NeRF and pose parameters. We highlight our approach in green.

TABLE I

RMSE OF THE TRANSLATIONAL ATE [M] ON TUM RGB-D [12]. THE UPPER ROWS ARE THE SLIGHTLY DYNAMIC SCENES AND THE LOWER ROWS ARE THE HIGHLY DYNAMIC SCENES. THE - DENOTES THAT NO RESULTS WERE REPORTED FOR THESE SEQUENCES.

Sequences	RGB-D					RGB				
	DVO-SLAM [38]	ORB-SLAM2 [17]	PointCorr [20]	DynaPix-D [37]	Yu et al. [24]	DytanVO [35]	DeFlowSLAM [21]	DROID-SLAM [16]	OURS (MS&SS)	OURS (MS)
fr2/desk-person	0.104	0.006	0.008	-	-	1.166	0.013	0.006	0.007	0.006
fr3/sitting-static	0.012	0.008	0.010	-	0.006	0.016	0.007	0.005	0.005	0.005
fr3/sitting-xyz	0.242	0.010	0.009	-	-	0.260	0.015	0.009	0.010	0.009
fr3/sitting-rpy	0.176	0.025	0.023	-	-	0.046	0.027	0.022	0.024	0.021
fr3/sitting-halfsphere	0.220	0.025	0.024	-	0.018	0.310	0.025	0.014	0.023	0.019
fr3/walking-static	0.752	0.408	0.011	0.007	0.009	0.021	0.007	0.012	0.007	0.014
fr3/walking-xyz	1.383	0.722	0.087	0.014	0.014	0.028	0.018	0.016	0.014	0.014
fr3/walking-rpy	1.292	0.805	0.161	0.123	0.031	0.155	0.057	0.040	0.031	0.039
fr3/walking-halfsphere	1.014	0.723	0.035	0.023	0.020	0.385	0.420	0.022	0.019	0.020
Mean/Max	0.577/1.383	0.304/0.805	0.041/0.161	-	-	0.265/1.166	0.065/0.420	0.016/0.040	0.016/0.031	0.016/0.039

found that setting the number of iterations for motion mask refinement to two provides stable convergence. For cases where the camera motion is higher than in the training sequences of DytanVO, the motion segmentation module results in an increase of false positives; as a counter-measure, we introduce a threshold of 60 % for the maximum amount of pixels that contain motion. Consequently, masks exceeding this threshold are discarded to ensure that there are always enough pixels for the dense bundle adjustment. Additionally, we only consider a pixel as dynamic if the confidence of the network exceeds 0.95 for the first and 0.98 for the remaining mask refinement steps.

While we use the reported image sizes for the novel view synthesis experiments, we use half of the resolution for the camera localization to be consistent with existent trajectory evaluations of DROID-SLAM [16].

Regarding the loss function, we set λ_{TV} initially to 0.005 and the number of sampled rays $|\mathcal{R}|$ per batch to 1024. We employ the default optimization settings for the dynamic

NeRF from [4] and use a multi-step learning rate decay scheduler for the pose refinement. The initial learning rate for the scheduler is set to $1 * 10^{-5}$ at the beginning of each pose optimization cycle and decayed every 1000 iterations by a factor of 0.9. As described beforehand, the actual used learning rate of the optimizer is retrieved by multiplication with the percentage of static pixels in the image. The number of optimization iterations is set to 200 000, unless otherwise stated.

To compare our camera pose retrieval with the classic way of using COLMAP, we follow the implementation of InstantNGP [3] to retrieve the COLMAP ground truth. Besides the COLMAP comparison, we compare our approach with RoDynRF [34]. For the TUM RGB-D dataset, we train their approach on an NVIDIA RTX 3090 with 24GB of VRAM. We follow their training guideline and do not employ prior pose initialization.

TABLE II

RMSE OF THE TRANSLATIONAL ATE [M] ON BONN RGB-D DYNAMIC [13]. RGB-D RESULTS ARE REPORTED BY PALAZZOLO ET AL. [13]. FOR DROID-SLAM AND OURS, WE CALCULATED THE RESULTS.

Sequences	RGB-D				RGB		
	ReFusion [13]	StaticFusion [41]	DynaSLAM (G) [23]	DynaSLAM (N+G) [23]	DROID-SLAM [16]	OURS (MS&SS)	OURS (MS)
balloon	0.175	0.233	0.050	0.030	0.075	0.028	0.068
balloon2	0.254	0.293	0.142	0.029	0.041	0.027	0.038
balloon_tracking	0.302	0.221	0.156	0.049	0.035	0.034	0.036
balloon_tracking2	0.322	0.366	0.192	0.035	0.026	0.032	0.028
crowd	0.204	3.586	1.065	0.016	0.052	0.035	0.061
crowd2	0.155	0.215	1.217	0.031	0.065	0.028	0.056
crowd3	0.137	0.168	0.835	0.038	0.046	0.032	0.055
kidnapping_box	0.148	0.336	0.026	0.029	0.020	0.021	0.020
kidnapping_box2	0.161	0.263	0.033	0.035	0.017	0.017	0.017
moving_no_box	0.071	0.141	0.317	0.232	0.023	0.013	0.014
moving_no_box2	0.179	0.364	0.052	0.039	0.040	0.027	0.026
moving_o_box	0.343	0.331	0.544	0.044	0.177	0.152	0.167
moving_o_box2	0.528	0.309	0.589	0.263	0.236	0.175	0.176
person_tracking	0.289	0.484	0.714	0.061	0.043	0.148	0.024
person_tracking2	0.463	0.626	0.817	0.078	0.054	0.022	0.035
placing_no_box	0.106	0.125	0.645	0.575	0.078	0.021	0.018
placing_no_box2	0.141	0.177	0.027	0.021	0.030	0.020	0.020
placing_no_box3	0.174	0.256	0.327	0.058	0.025	0.022	0.022
placing_o_box	0.571	0.330	0.267	0.255	0.127	0.172	0.117
removing_no_box	0.041	0.136	0.016	0.016	0.016	0.015	0.015
removing_no_box2	0.111	0.129	0.022	0.021	0.020	0.019	0.021
removing_o_box	0.222	0.334	0.362	0.291	0.189	0.177	0.181
synchronous	0.441	0.446	0.977	0.015	0.006	0.007	0.006
synchronous2	0.022	0.027	0.887	0.009	0.012	0.006	0.011
Mean/Max	0.232/0.571	0.412/3.586	0.428/1.217	0.095/0.575	0.061/0.236	0.052/ 0.177	0.051 /0.181

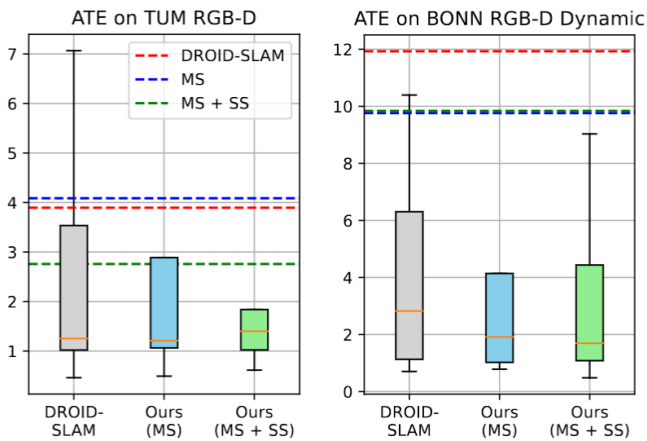


Fig. 3. RMSE of the rotational ATE [°] on the TUM RGB-D dataset (left) and the BONN RGB-D Dynamic dataset (right). The median is shown in orange and the average in dotted lines.

C. Camera Localization Quality

Our results on all datasets show a lower translational trajectory error compared to state-of-the-art approaches, see Table I and Table II. We compare RGB-D-based and monocular SLAM approaches with our proposed camera retrieval method using only motion masks (MS) as well as using motion and semantic segmentation masks in combination (MS&SS). Looking at the mean value of the RMSE of the translational trajectory error over all sequences, our approach performs similarly to DROID-SLAM on TUM RGB-D. However, the maximum error value is much lower,

TABLE III

NOVEL VIEW SYNTHESIS RESULTS ON TUM RGB-D [12]. THE UPPER ROWS ARE THE SLIGHTLY DYNAMIC SCENES AND THE LOWER ROWS ARE THE HIGHLY DYNAMIC SCENES. THE - DENOTES THAT THE CAMERA POSE COULD NOT BE REGRESSED.

Sequences	RGB-D		RGB	
	RoDynRF	HexPlane (COLMAP)	HexPlane + DynaMoN Backbone (Ours)	DynaMoN (Ours)
fr2/desk-person	6.05 / 0.127	-	23.04 / 0.680	24.83 / 0.725
fr3/sitting-static	9.67 / 0.123	-	28.55 / 0.899	28.95 / 0.903
fr3/sitting-xyz	10.10 / 0.150	19.98 / 0.589	25.90 / 0.848	26.15 / 0.850
fr3/sitting-rpy	8.35 / 0.121	16.63 / 0.472	25.76 / 0.843	26.40 / 0.853
fr3/sitting-halfsphere	7.46 / 0.157	24.25 / 0.793	24.05 / 0.792	24.60 / 0.799
fr3/walking-static	10.01 / 0.159	20.27 / 0.650	25.84 / 0.849	26.25 / 0.853
fr3/walking-xyz	10.02 / 0.171	-	24.05 / 0.797	24.34 / 0.796
fr3/walking-rpy	8.81 / 0.201	-	24.18 / 0.790	24.70 / 0.796
fr3/walking-halfsphere	8.79 / 0.205	22.01 / 0.692	24.05 / 0.781	24.27 / 0.779
Mean	8.84 / 0.157	-	25.05 / 0.809	25.60 / 0.819

which shows that it is less prone to failure when applied to real-world scenarios. Moreover, comparing the RMSE of the rotational ATE, see Figure 3, our MS&SS-model achieves lower values than DROID-SLAM. On the BONN RGB-D Dynamic dataset, our approach outperforms the state-of-the-art approaches in terms of mean and maximum trajectory error for both rotation and translation.

D. Novel View Synthesis Quality

To evaluate our approach from a NeRF perspective we consider two aspects. First, the traditional way of generating camera ground truth when using NeRF is the use of COLMAP. Thus, we compare DynaMoN with HexPlane [4]



Fig. 4. **Qualitative Results for Novel View Synthesis** on TUM RGB-D dataset (top) and BONN RGB-D Dynamic dataset (bottom). Shown are original Ground Truth images (left) and synthesized views from COLMAP-based dynamic NeRF (2nd column) with improved camera poses from our backbone (3rd column) only, and our full model (right).

TABLE IV

NOVEL VIEW SYNTHESIS RESULTS ON BONN RGB-D DYNAMIC [13].
THE - DENOTES THAT THE CAMERA POSE COULD NOT BE REGRESSED.

PSNR↑/SSIM↑	RGB		
	HexPlane (COLMAP)	HexPlane + DynaMoN Backbone (Ours)	DynaMoN (Ours)
Sequences			
balloon	-	29.83 / 0.868	29.84 / 0.866
balloon2	-	27.61 / 0.841	28.31 / 0.847
balloon_tracking	-	29.27 / 0.847	29.55 / 0.846
balloon_tracking2	-	29.68 / 0.860	30.56 / 0.862
crowd	-	27.92 / 0.831	28.40 / 0.829
crowd2	-	26.68 / 0.825	27.97 / 0.827
crowd3	-	26.57 / 0.815	27.40 / 0.827
kidnapping_box	-	30.43 / 0.870	30.59 / 0.869
kidnapping_box2	-	30.28 / 0.860	30.18 / 0.857
moving_no_box	30.67 / 0.881	30.32 / 0.866	30.36 / 0.862
moving_no_box2	31.14 / 0.890	30.57 / 0.874	30.62 / 0.870
moving_o_box	29.21 / 0.889	30.26 / 0.884	31.08 / 0.888
moving_o_box2	-	29.82 / 0.875	29.40 / 0.875
person_tracking	26.57 / 0.808	27.78 / 0.843	28.71 / 0.845
person_tracking2	-	27.47 / 0.837	27.80 / 0.833
placing_no_box	25.73 / 0.780	30.94 / 0.869	31.23 / 0.870
placing_no_box2	-	31.18 / 0.885	31.45 / 0.884
placing_no_box3	-	30.79 / 0.879	30.83 / 0.875
placing_o_box	-	30.42 / 0.886	31.12 / 0.890
removing_no_box	-	30.66 / 0.879	30.85 / 0.877
removing_no_box2	31.13 / 0.887	30.73 / 0.871	30.86 / 0.870
removing_o_box	31.13 / 0.887	30.30 / 0.880	30.76 / 0.882
synchronous	-	28.42 / 0.835	28.93 / 0.834
synchronous2	-	28.85 / 0.887	30.18 / 0.891
Mean	-	29.45 / 0.861	29.87 / 0.861

using camera poses from COLMAP. Second, we highlight the influence of the iterative pose refinement by training both DynaMoN and HexPlane with our initially localized poses. Third, we compare our approach with RoDynRF [34] which

TABLE V

ANALYSIS OF THE INFLUENCE OF DIFFERENT POSE RETRIEVAL STEPS TO PSNR AND SSIM IN THE BONN RGB-D DYNAMIC CROWD2 SCENE WITH SPARSE INPUT TRAJECTORY.

Approach	PSNR↑/SSIM↑
DROID-SLAM [16] + HexPlane [4]	16.46 / 0.661
Our initial poses + HexPlane [4]	17.07 / 0.660
DynaMoN (Ours)	17.31 / 0.659

regresses the camera pose along with a dynamic NeRF.

The results for the TUM RGB-D dataset are denoted in Table III. DynaMoN leads to a higher novel view synthesis quality compared to HexPlane without refined poses, RoDynRF, and when using COLMAP for the camera poses. Qualitative examples of our renderings are shown in Fig. 4.

On the BONN RGB-D Dynamic dataset, COLMAP is challenged on several sequences (cf. Tab. IV). DynaMoN can retrieve camera poses for all scenes (Tab. II) and performs well on novel view synthesis for all sequences (Tab. IV). In addition, the PSNR is increased by the alternating training scheme. However, for the cases where COLMAP succeeds in the pose estimation, the camera poses from SfM also lead to decent novel view synthesis results. Examples of renderings can be seen in Fig. 4.

E. Robustness on Sparse Trajectories

In this section, we evaluate the robustness of different parts of our pose retrieval when faced with a dynamic and sparse trajectory. Using only every tenth frame of the crowd2 sequence, we show how the DROID-SLAM poses compare to the ones from the dynamics-masked camera pose retrieval and our neural camera pose refinement in terms of novel

TABLE VI

ANALYSIS OF THE RUNTIME ON THE TUM RGB-D fr2/DESK-PERSON SCENE. ‡ MEANS 100 000 TRAINING ITERATIONS AND A BATCH SIZE OF 512.

† MEANS 100 000 TRAINING ITERATIONS AND A BATCH SIZE OF 1 024. THE TIME FORMAT IS HOURS:MINUTES:SECONDS.

Approach	Pre-processing time↓	Training time↓	Rendering time↓	Total time↓	PSNR↑/SSIM↑
RoDynRF [34] ‡	01:52:55	08:00:44	00:11:15	10:04:54	6.05 / 0.127
DynaMoN (Ours)	00:13:49	09:49:25	00:42:32	10:45:46	24.83 / 0.725
DynaMoN (Ours) †	00:14:12	05:04:19	00:42:20	06:00:51	23.95 / 0.702
DynaMoN (Ours) ‡	00:13:41	04:43:23	01:03:21	06:00:25	23.43 / 0.690

view rendering quality. Looking at the PSNR values in Table V, it can be noted that each of our proposed components incrementally increases the reconstruction quality. Thus, when confronted with a sparse trajectory of a highly dynamic scene, DynaMoN outperforms pure DROID-SLAM making it more robust to realistic, real-world scenarios with imperfect camera recordings.

F. Runtime and Memory Evaluation

Finally, the runtime of DynaMoN is measured and the memory requirements are mentioned. Both are presented in comparison with RoDynRF [34] on a workstation with an NVIDIA RTX 4090 graphics card with 24 gigabytes of video random-access memory (VRAM). We report the results for the TUM RGB-D fr2/desk-person sequence in Table VI as it is by far the longest scene of both datasets comprising 4067 frames. In terms of memory requirement, RoDynRF can only be trained with a batch size of 512 in this setting, while DynaMoN is more memory-efficient, enabling a batch size of 1024. From the experiments, it can be concluded that the total time for pre-processing, training and rendering of DynaMoN is comparable to RoDynRF if the default training strategy with 200000 iterations is utilized. However, if our model is trained for 100000 iterations which is the default value of RoDynRF, the total time can be greatly reduced without a significant drop in photometric accuracy. For this shorter training, the NeRF and pose optimization of DynaMoN alternate every 2500 iterations. Furthermore, a decrease of the batch size to the same value as in the competitor method further speeds up the training time at the cost of a longer rendering time while staying comparably accurate. It has to be noted that the pre-processing of RoDynRF consisting of monocular depth prediction, optical flow prediction, motion mask generation and dataloading takes about eight times longer than our pre-processing loading the data and generating initial poses as well as motion masks.

V. DISCUSSION

In comparison to traditional sparse reconstructions [15], [14], [16], our approach addresses camera localization and dynamic novel view synthesis in combination. While this leads to more pleasing 3D visualizations and novel view synthesis results, the computing time is higher compared to traditional camera localization and non-dynamic 3D representation methods [9], [10], [11]. Nevertheless, compared to combined dynamic camera localization and dynamic novel view synthesis approaches [34], our approach requires only

60% of the training time when using the same number of iterations and batch size, while being more robust in more dynamic scenes with dynamic camera motion.

Moreover, our approach shows an improved performance compared to the state-of-the-art for camera localization. Only using our motion masks already improves the performance. Moreover, for scenes with large motions, the combination with semantic segmentation masks provides significantly improved camera localization results.

The results presented in Table III indicate that RoDynRF [34], despite being a state-of-the-art method that integrates combined camera regression with novel view synthesis, faces significant challenges in handling highly dynamic camera movements and dynamic scenes. In contrast, our method demonstrates superior robustness and yields improved outcomes when compared to both RoDynRF [34] and HexPlane [4] employing COLMAP poses on the demanding TUM RGB-D dataset. Furthermore, our iterative pose refinement process enhances robustness, as evidenced in Table V, and achieves better performance in novel view synthesis on both datasets.

VI. CONCLUSION

We present DynaMoN, a motion-aware fast and robust camera localization approach for novel view synthesis. DynaMoN can handle not only the motion of known objects using semantic segmentation masks but also that of unknown objects using a motion segmentation mask. Furthermore, it retrieves camera poses faster and is more robust to scene dynamics in comparison to traditional SfM approaches, enabling a more accurate 4D scene representation. In addition, DynaMoN is trained with a novel iterative training scheme that refines NeRF parameters and the initially provided poses in an alternating fashion. Compared to the state-of-the-art, DynaMoN outperforms other dynamic camera localization approaches and shows better results for novel view synthesis on scenes with high camera motion.

ACKNOWLEDGMENT

We thank d.hip for providing a campus stipend.

REFERENCES

- [1] M. Broxton, J. Flynn, R. Overbeck, D. Erickson, P. Hedman, M. Duvall, J. Dourgarian, J. Busch, M. Whalen, and P. Debevec, "Immersive light field video with a layered mesh representation," *ACM Trans. Graph.*, vol. 39, no. 4, aug 2020.
- [2] A. Rosinol, J. J. Leonard, and L. Carlone, "Nerf-slam: Real-time dense monocular slam with neural radiance fields," *arXiv preprint arXiv:2210.13641*, 2022.

- [3] T. Müller, A. Evans, C. Schied, and A. Keller, "Instant neural graphics primitives with a multiresolution hash encoding," *ACM Transactions on Graphics (ToG)*, vol. 41, no. 4, pp. 1–15, 2022.
- [4] A. Cao and J. Johnson, "Hexplane: A fast representation for dynamic scenes," in *Proceedings of the IEEE/CVF Conference on Computer Vision and Pattern Recognition*, 2023, pp. 130–141.
- [5] R. Shao, Z. Zheng, H. Tu, B. Liu, H. Zhang, and Y. Liu, "Tensor4d: Efficient neural 4d decomposition for high-fidelity dynamic reconstruction and rendering," in *Proceedings of the IEEE/CVF Conference on Computer Vision and Pattern Recognition*, 2023, pp. 16 632–16 642.
- [6] L. Song, A. Chen, Z. Li, Z. Chen, L. Chen, J. Yuan, Y. Xu, and A. Geiger, "Nerfplayer: A streamable dynamic scene representation with decomposed neural radiance fields," *IEEE Transactions on Visualization and Computer Graphics*, pp. 2732–2742, 2023.
- [7] J. Fang, T. Yi, X. Wang, L. Xie, X. Zhang, W. Liu, M. Nießner, and Q. Tian, "Fast dynamic radiance fields with time-aware neural voxels," in *SIGGRAPH Asia 2022 Conference Papers*, 2022.
- [8] J. L. Schonberger and J.-M. Frahm, "Structure-from-motion revisited," in *Proceedings of the IEEE conference on computer vision and pattern recognition*, 2016, pp. 4104–4113.
- [9] Z. Zhu, S. Peng, V. Larsson, W. Xu, H. Bao, Z. Cui, M. R. Oswald, and M. Pollefeys, "Nice-slam: Neural implicit scalable encoding for slam," in *Proceedings of the IEEE/CVF Conference on Computer Vision and Pattern Recognition*, 2022, pp. 12 786–12 796.
- [10] Z. Zhu, S. Peng, V. Larsson, Z. Cui, M. R. Oswald, A. Geiger, and M. Pollefeys, "Nicer-slam: Neural implicit scene encoding for rgb slam," *arXiv preprint arXiv:2302.03594*, 2023.
- [11] C.-M. Chung, Y.-C. Tseng, Y.-C. Hsu, X.-Q. Shi, Y.-H. Hua, J.-F. Yeh, W.-C. Chen, Y.-T. Chen, and W. H. Hsu, "Orbeez-slam: A real-time monocular visual slam with orb features and nerf-realized mapping," in *2023 IEEE International Conference on Robotics and Automation (ICRA)*. IEEE, 2023, pp. 9400–9406.
- [12] J. Sturm, N. Engelhard, F. Endres, W. Burgard, and D. Cremers, "A benchmark for the evaluation of rgb-d slam systems," in *Proc. of the International Conference on Intelligent Robot Systems (IROS)*, 2012.
- [13] E. Palazzolo, J. Behley, P. Lottes, P. Giguère, and C. Stachniss, "ReFusion: 3D Reconstruction in Dynamic Environments for RGB-D Cameras Exploiting Residuals," in *2019 IEEE/RSJ International Conference on Intelligent Robots and Systems (IROS)*. IEEE, 2019, pp. 7855–7862.
- [14] R. Mur-Artal, J. M. M. Montiel, and J. D. Tardos, "Orb-slam: a versatile and accurate monocular slam system," *IEEE transactions on robotics*, vol. 31, no. 5, pp. 1147–1163, 2015.
- [15] J. Campos, R. Elvira, J. J. G. Rodríguez, J. M. Montiel, and J. D. Tardós, "Orb-slam3: An accurate open-source library for visual, visual-inertial, and multimap slam," *IEEE Transactions on Robotics*, vol. 37, no. 6, pp. 1874–1890, 2021.
- [16] Z. Teed and J. Deng, "Droid-slam: Deep visual slam for monocular, stereo, and rgb-d cameras," *Advances in neural information processing systems*, vol. 34, pp. 16 558–16 569, 2021.
- [17] R. Mur-Artal and J. D. Tardós, "Orb-slam2: An open-source slam system for monocular, stereo, and rgb-d cameras," *IEEE transactions on robotics*, vol. 33, no. 5, pp. 1255–1262, 2017.
- [18] C. Yu, Z. Liu, X.-J. Liu, F. Xie, Y. Yang, Q. Wei, and Q. Fei, "Ds-slam: A semantic visual slam towards dynamic environments," in *2018 IEEE/RSJ International conference on intelligent robots and systems (IROS)*. IEEE, 2018, pp. 1168–1174.
- [19] M. Henein, J. Zhang, R. Mahony, and V. Ila, "Dynamic slam: The need for speed," in *2020 IEEE International Conference on Robotics and Automation (ICRA)*. IEEE, 2020, pp. 2123–2129.
- [20] W. Dai, Y. Zhang, P. Li, Z. Fang, and S. Scherer, "Rgb-d slam in dynamic environments using point correlations," *IEEE Transactions on Pattern Analysis and Machine Intelligence*, vol. 44, no. 1, pp. 373–389, 2020.
- [21] W. Ye, X. Yu, X. Lan, Y. Ming, J. Li, H. Bao, Z. Cui, and G. Zhang, "Deflow-slam: Self-supervised scene motion decomposition for dynamic dense slam," *arXiv preprint arXiv:2207.08794*, 2022.
- [22] M. Runz, M. Buffier, and L. Agapito, "Maskfusion: Real-time recognition, tracking and reconstruction of multiple moving objects," in *2018 IEEE International Symposium on Mixed and Augmented Reality (ISMAR)*. IEEE, 2018, pp. 10–20.
- [23] B. Bescos, J. M. Fàcil, J. Civera, and J. Neira, "Dynaslam: Tracking, mapping, and inpainting in dynamic scenes," *IEEE Robotics and Automation Letters*, vol. 3, no. 4, pp. 4076–4083, 2018.
- [24] X. Yu, R. Shen, K. Wu, and Z. Lin, "Robust visual slam in dynamic environment based on motion detection and segmentation," *Journal of Autonomous Vehicles and Systems*, 2024. [Online]. Available: <https://api.semanticscholar.org/CorpusID:270957414>
- [25] B. Mildenhall, P. P. Srinivasan, M. Tancik, J. T. Barron, R. Ramamoorthi, and R. Ng, "Nerf: Representing Scenes as Neural Radiance Fields for View Synthesis," in *European Conference on Computer Vision*. Springer, 2020, pp. 405–421.
- [26] E. Sucar, S. Liu, J. Ortiz, and A. J. Davison, "imap: Implicit mapping and positioning in real-time," in *Proceedings of the IEEE/CVF International Conference on Computer Vision*, 2021, pp. 6229–6238.
- [27] A. Pumarola, E. Corona, G. Pons-Moll, and F. Moreno-Noguer, "D-nerf: Neural radiance fields for dynamic scenes," in *Proceedings of the IEEE/CVF Conference on Computer Vision and Pattern Recognition*, 2021, pp. 10 318–10 327.
- [28] K. Park, U. Sinha, J. T. Barron, S. Bouaziz, D. B. Goldman, S. M. Seitz, and R. Martin-Brualla, "Nerfies: Deformable neural radiance fields," in *Proceedings of the IEEE/CVF International Conference on Computer Vision*, 2021, pp. 5865–5874.
- [29] Z. Wang, S. Wu, W. Xie, M. Chen, and V. A. Prisacariu, "NeRF-: Neural radiance fields without known camera parameters," *arXiv preprint arXiv:2102.07064*, 2021.
- [30] Q. Meng, A. Chen, H. Luo, M. Wu, H. Su, L. Xu, X. He, and J. Yu, "GNerF: GAN-Based Neural Radiance Field Without Posed Camera," in *Proceedings of the IEEE/CVF International Conference on Computer Vision (ICCV)*, Oct. 2021, pp. 6351–6361.
- [31] L. Yen-Chen, P. Florencie, J. T. Barron, A. Rodriguez, P. Isola, and T.-Y. Lin, "iNeRF: Inverting Neural Radiance Fields for Pose Estimation," in *2021 IEEE/RSJ International Conference on Intelligent Robots and Systems (IROS)*, 2021, pp. 1323–1330.
- [32] W. Bian, Z. Wang, K. Li, J.-W. Bian, and V. A. Prisacariu, "Nope-nerf: Optimising neural radiance field with no pose prior," in *Proceedings of the IEEE/CVF Conference on Computer Vision and Pattern Recognition*, 2023, pp. 4160–4169.
- [33] H. Schieber, F. Deuser, B. Egger, N. Oswald, and D. Roth, "Nerfrinsic four: An end-to-end trainable nerf jointly optimizing diverse intrinsic and extrinsic camera parameters," 2023.
- [34] Y.-L. Liu, C. Gao, A. Meuleman, H.-Y. Tseng, A. Saraf, C. Kim, Y.-Y. Chuang, J. Kopf, and J.-B. Huang, "Robust dynamic radiance fields," in *Proceedings of the IEEE/CVF Conference on Computer Vision and Pattern Recognition*, 2023, pp. 13–23.
- [35] S. Shen, Y. Cai, W. Wang, and S. Scherer, "Dytanvo: Joint refinement of visual odometry and motion segmentation in dynamic environments," in *2023 IEEE International Conference on Robotics and Automation (ICRA)*. IEEE, 2023, pp. 4048–4055.
- [36] A. Chen, Z. Xu, A. Geiger, J. Yu, and H. Su, "Tensorf: Tensorial radiance fields," in *European Conference on Computer Vision*. Springer, 2022, pp. 333–350.
- [37] C. Xu, E. Bonetto, and A. Ahmad, "Dynapix slam: A pixel-based dynamic slam approach," *arXiv preprint arXiv:2309.09879*, 2023.
- [38] C. Kerl, J. Sturm, and D. Cremers, "Robust odometry estimation for rgb-d cameras," in *2013 IEEE international conference on robotics and automation*. IEEE, 2013, pp. 3748–3754.
- [39] Z. Zhang and D. Scaramuzza, "A tutorial on quantitative trajectory evaluation for visual (-inertial) odometry," in *2018 IEEE/RSJ International Conference on Intelligent Robots and Systems (IROS)*. IEEE, 2018, pp. 7244–7251.
- [40] Z. Wang, A. C. Bovik, H. R. Sheikh, and E. P. Simoncelli, "Image quality assessment: from error visibility to structural similarity," *IEEE transactions on image processing*, vol. 13, no. 4, pp. 600–612, 2004, publisher: IEEE.
- [41] R. Scona, M. Jaimez, Y. R. Petillot, M. Fallon, and D. Cremers, "Staticfusion: Background reconstruction for dense rgb-d slam in dynamic environments," in *2018 IEEE international conference on robotics and automation (ICRA)*. IEEE, 2018, pp. 3849–3856.
- [42] L.-C. Chen, G. Papandreou, F. Schroff, and H. Adam, "Rethinking atrous convolution for semantic image segmentation," *arXiv preprint arXiv:1706.05587*, 2017.
- [43] K. He, X. Zhang, S. Ren, and J. Sun, "Deep residual learning for image recognition," in *Proceedings of the IEEE conference on computer vision and pattern recognition*, 2016, pp. 770–778.
- [44] T.-Y. Lin, M. Maire, S. Belongie, J. Hays, P. Perona, D. Ramanan, P. Dollár, and C. L. Zitnick, "Microsoft coco: Common objects in context," in *Computer Vision—ECCV 2014: 13th European Conference*,

Zurich, Switzerland, September 6-12, 2014, Proceedings, Part V 13.
Springer, 2014, pp. 740–755.